A moving wave probe reveals a friction kernel hidden by phase averaging in turbulence

Guoqiang Liu[1,*] and Maryam Al Alshehhi[1]

[1] *Department of Civil, Infrastructural and Environmental Engineering, Khalifa University of Science and Technology, Abu Dhabi, UAE*

(Dated: April 16, 2026)

Coarse-graining routinely discards fluctuations whose one-time mean vanishes, yet irreversible transport is controlled by two-time correlations. Here we introduce a moving-probe protocol that detects transport channels hidden by this discard operation. A prescribed wave-like carrier isolates a chosen bilinear coupling in a stochastic bath. Three falsifiable controls distinguish genuine Green–Kubo signal from spurious response. We apply the protocol to the stochastic vortex force, the bilinear wave-vorticity coupling eliminated by classical phase averaging in wave–current theory. In Navier–Stokes isotropic turbulence at $\mathrm{Re}_\lambda \approx 433$, the probe yields a finite friction kernel. A phase-averaging surrogate suppresses it to the shuffled-noise baseline, time shuffling destroys temporal memory, and a detuned control reduces the signal by more than two orders of magnitude. Trajectory sampling shows that probe motion shortens the decorrelation time toward the independent-encounter limit. The protocol demonstrates that coarse-graining can hide a real transport channel and that an actively prescribed probe makes the channel operationally measurable.

Introduction.—Effective theories are built by discarding fluctuations. The usual justification is simple. If a fluctuation has zero mean, it should not contribute systematically at large scales. But irreversible transport is controlled by two-time correlations, not by one-time averages alone [1–5]. A fluctuation whose instantaneous mean vanishes can still carry a finite Green–Kubo coefficient and therefore a finite friction channel. This raises a sharp question. Can a specific coarse-graining step erase a specific transport channel that is physically present in the underlying Navier–Stokes dynamics?

That question is difficult because a Green–Kubo measurement in turbulence is usually generic. It probes whatever correlations happen to be present in the flow, not a targeted coupling channel. To demonstrate channel suppression, one must separately establish three facts. The channel carries a finite kernel. The kernel is specific to that channel rather than generic to turbulence. And the coarse-graining step of interest is what removes it. Without a channel-selective probe, these three statements remain entangled.

Here we introduce an active strategy rather than a passive diagnostic. We prescribe a moving wave-like carrier inside the turbulent flow, using it as a kinematic probe that selects a specific bilinear coupling channel. The probe does not attempt to solve the full coupled wave–turbulence problem. Instead, it inserts the wave-side reference structure needed to ask a cleaner question. If turbulence is interrogated by a moving wave, does a finite friction kernel emerge from the targeted coupling? And is that kernel precisely what phase averaging removes? The strategy is indifferent to the specific wave type, bath dynamics, or closure scheme. It applies whenever coarse-graining eliminates a bilinear coupling between a fast wave and a slow stochastic bath.

We apply this idea to the stochastic vortex force (SVF) $\boldsymbol{f}_{\mathrm{svf}} = \boldsymbol{u}_\phi \times \boldsymbol{\omega}'$, the bilinear coupling between wave orbital motion and turbulent vorticity fluctuations [6–10]. In classical wave–current theory this term is eliminated by phase averaging because its phase mean vanishes. The Craik–Leibovich vortex force survives and drives Langmuir circulation [11]. The SVF does not survive. Yet its two-time autocorrelation need not vanish, and if finite, it defines a friction kernel. Reference [12] shows that, under Kolmogorov closure, this channel yields the parameter-free ocean swell attenuation law

$$\mu_E = C_{\mathrm{tot}} \varepsilon^{2/3} g^{-7/3} \omega^{8/3}, \qquad C_{\mathrm{tot}} = 2\pi/3. \tag{1}$$

That work validates the macroscopic output against 241 trans-oceanic satellite swell tracks [13–16]. The missing question is whether the kernel itself can be exposed directly inside Navier–Stokes turbulence.

Our central result is that it can. The moving wave probe reveals a finite Green–Kubo friction kernel in Navier–Stokes turbulence at $\mathrm{Re}_\lambda \approx 433$. A phase-averaging surrogate suppresses the matched kernel to the shuffled-noise baseline. Time shuffling destroys it entirely. A detuned control shows that the large signal is not generic to arbitrary probe choices. The result is not merely that turbulence has memory, but that a transport channel hidden by coarse-graining can be made directly measurable by an actively prescribed probe.

We use two sampling configurations. Fixed-point sampling retrieves vorticity time series at 200 stationary positions and tests existence, channel specificity, and phase-averaging suppression. Trajectory sampling moves the probe through the turbulence at speed c_g and tests sweep-influenced decorrelation, encounter independence, and single-encounter statistics.

DNS dataset.—All measurements use the `isotropic1024coarse` dataset from the Johns Hopkins Turbulence Database [17, 18]. It is forced homogeneous isotropic turbulence on a 1024^3 grid with $\mathrm{Re}_\lambda \approx 433$. The dissipation rate is $\varepsilon = 0.093$. The kinematic viscos-

ity is $\nu = 1.85 \times 10^{-4}$. The periodic box has side 2π. The dataset contains 5028 frames with uniform spacing $\Delta t = 0.002$ over $t \in [0, 10.056]$. We query the velocity gradient tensor $\partial u_i/\partial x_j$ through pyJHTDB on SciServer with fourth-order Lagrange spatial interpolation and piecewise cubic Hermite temporal interpolation. The vorticity is computed as $\omega_i' = \epsilon_{ijk}\partial_j u_k$.

Kinematic probe.—At each sampling location $\boldsymbol{x}$ we prescribe

$$\boldsymbol{u}_\phi(\boldsymbol{x}, t) = U_0 \cos(kx - \omega t)\, \hat{\boldsymbol{x}}, \tag{2}$$

where U_0 is the probe velocity amplitude, k is the probe wavenumber, $\omega = \sqrt{g_{\mathrm{ref}} k}$ is the probe frequency, and $\hat{\boldsymbol{x}}$ is the propagation direction. The associated group speed is $c_g = g_{\mathrm{ref}}/(2\omega)$. We define the coupling parameter $\delta(k) = u'(k)/c_g(k)$, where $u'(k)$ is the band-passed turbulent velocity at scale k. The probe amplitude is vertically uniform. We do not apply depth weighting e^{kz}, avoiding artificial vertical inhomogeneity in the sampled DNS bath. The SVF force $\boldsymbol{f}_{\mathrm{svf}} = \boldsymbol{u}_\phi \times \boldsymbol{\omega}'$ has nonzero components

$$f_y = -U_0 \cos\varphi\, \omega_z', \qquad f_z = U_0 \cos\varphi\, \omega_y', \qquad \varphi = kx - \omega t. \tag{3}$$

The mode-projected force is

$$F_k(t) = e^{-i\varphi}\big(f_y + i f_z\big). \tag{4}$$

Although $\boldsymbol{u}_\phi \cdot (\boldsymbol{u}_\phi \times \boldsymbol{\omega}') = 0$ pointwise, the relevant observable is not local power but the modal work $\mathrm{d}E_k/\mathrm{d}t = \mathrm{Re}\,[a_k^* F_k]$, with a_k the complex probe-mode amplitude.

Autocorrelation and operational demodulation.—We compute $C_F(\tau) = \langle F_k(0) F_k^*(\tau)\rangle$ by FFT using the Wiener–Khinchin theorem and average over positions and time origins. For the present one-component probe,

$$F_k(t) \propto \frac{1 + e^{-2i\varphi(t)}}{2}\, W(t), \qquad W(t) = -\omega_z'(t) + i\omega_y'(t). \tag{5}$$

After ensemble averaging, the surviving carrier term in $\mathrm{Re}\, C_F(\tau)$ is proportional to $1 + \cos(2\omega\tau) = 2\cos^2(\omega\tau)$. This is carrier self-mixing from the one-component probe, not physical bath decorrelation. The missing quadrature partner $\sin\varphi$ would complete circular polarisation and cancel this residual analytically. The Hilbert envelope used here removes this artifact operationally. It is not an arbitrary signal-processing step. We define the encounter duration from the smoothed Hilbert envelope $\mathcal{E}(\tau)$ of the normalized real part of C_F,

$$\tau_{\mathrm{int}} = \int_0^{\tau_{\mathrm{env}}} \mathcal{E}(\tau)\, \mathrm{d}\tau, \tag{6}$$

where τ_{env} is the first time at which the smoothed envelope falls below 0.05. Sensitivity to smoothing and threshold choice is documented in the Supplemental Material [19].

In the present DNS, $\tau_{\mathrm{env}}/T_{\mathrm{wave}} \approx 10$–$17$, so many carrier cycles remain visible inside the decorrelation window. Demodulation is therefore operationally necessary. Under oceanic parameters, $\tau_c/T_{\mathrm{wave}} \approx 1/\pi < 1$, so the carrier would not complete a full cycle before the envelope decays and demodulation would matter much less.

We define the Eulerian Green–Kubo coefficient by

$$\Gamma_{\mathrm{GK}}^{\mathrm{Eul}} = \frac{1}{2E_k} \int_0^{\tau_{\mathrm{env}}} \mathrm{Re}\, C_F(\tau)\, \mathrm{d}\tau, \qquad E_k = \tfrac{1}{2} U_0^2. \tag{7}$$

In the fast-carrier regime $\omega\tau_c \gg 1$, where $\cos^2(\omega\tau)$ averages to $1/2$ across the decorrelation window, this coefficient becomes proportional to the Euler-frame zero-frequency spectral density of the single-component vorticity process. That identification is approximate. It relies on the fast-carrier regime, envelope truncation in place of the infinite-time integral, and position averaging to suppress cross-terms. It integrates over all spatial wavenumbers q and is therefore not directly comparable to the theoretical prefactor $C_{\mathrm{tot}} = 2\pi/3$, which involves only the resonant band $q \sim k$ weighted by the sweep-decorrelation kernel $\mathcal{W}(q/k)$. $\Gamma_{\mathrm{GK}}^{\mathrm{Eul}}$ should be read as an existence diagnostic for the selected channel, not as a direct estimate of the oceanic attenuation coefficient μ_E.

Encounter partition.—Each $F_k(t)$ record is partitioned into non-overlapping segments of duration τ_{int}. The per-encounter increment is

$$\xi_n = \frac{1}{E_k} \int_{t_n}^{t_n + \tau_{\mathrm{int}}} \mathrm{Re}[U_0^* F_k(t)]\, \mathrm{d}t. \tag{8}$$

Because U_0 is fixed and $\langle F_k\rangle = 0$, the kinematic probe enforces $\langle \xi\rangle = 0$ by construction. It can diagnose encounter variance, serial correlation, and higher moments, but cannot generate mean wave-energy drift. The encounter-to-encounter correlation function is $C_\xi(m) = \langle \xi_n \xi_{n+m}\rangle / \langle \xi^2\rangle$, and the closure parameter is $c_0 = 1 + 2\sum_{m\geq 1} C_\xi(m)$. Independent encounters give $c_0 = 1$.

Fixed-point configuration.—We sample $N_p = 200$ positions drawn uniformly from $(0.1, 2\pi - 0.1)^3$. We use three probe wavenumbers $k \in \{10, 15, 30\}$ at fixed $g_{\mathrm{ref}} = 38\,269$, giving $\delta = 0.008$–0.010. These wavenumbers keep the probe frequency below 85% of the Nyquist frequency $\omega_N = \pi/\Delta t \approx 1571$.

Trajectory configuration.—The probe advances as $\boldsymbol{x}(t) = \boldsymbol{x}_0 + c_g t\, \hat{\boldsymbol{x}} \pmod{2\pi}$. We fix $k = 30$ and scan $\delta \in \{0.01, 0.03, 0.05, 0.1\}$ by varying $g_{\mathrm{ref}} \in \{38\,269,\ 4\,252,\ 1\,531,\ 383\}$, giving $c_g \in \{17.9,\ 6.0,\ 3.6,\ 1.8\}$. For each δ we launch 50 trajectories from independent random initial positions, giving 200 trajectories in total.

A moving wave probe reveals a hidden, memory-bearing friction kernel (Fig. 1).—We establish three properties by targeted controls on the 200-position fixed-point dataset. Main-text controls are shown at $k = 10$, where both the probe frequency and its first harmonic remain

below the Nyquist limit. The same ordering persists at higher k. Aliasing effects there are documented in Appendix .

Phase-averaging surrogate. The probe defines a reference frequency ω. For the SVF force $f_y = -U_0 \cos\varphi\, \omega'_z$, the carrier modulation $\cos\varphi$ shifts the broadband vorticity spectrum into sidebands centered on ω. Craik–Leibovich phase averaging removes the SVF identically because $\langle \cos\varphi \rangle_{\mathrm{phase}} = 0$ [6, 9]. To test whether the measured kernel depends on this carrier-sideband content, we approximate the removal by low-pass filtering $f_y(t)$ and $f_z(t)$ below 0.4ω before modal projection to F_k. By the modulation theorem, all SVF energy resides near ω. In the fast-carrier regime used here ($\omega \approx 619 \gg \omega_{\mathrm{turb}}$), the filter suppresses the matched content with only residual leakage through the Butterworth transition band. Even this approximate removal collapses the kernel to the shuffled-noise baseline [Fig. 1(a)], with $\Gamma_{\mathrm{GK}}^{\mathrm{Eul}\,\mathrm{surr}} / \Gamma_{\mathrm{GK}}^{\mathrm{Eul}\,\mathrm{SVF}} < 0.01$. The kernel is therefore carried by the spectral content that phase averaging would eliminate.

Time shuffling. We randomly permute the time indices of the $F_k(t)$ series. This preserves $P(F_k)$ and destroys all temporal structure. After shuffling, the autocorrelation drops to the shuffled-noise baseline for $\tau > 0$, and the Green–Kubo integral is strongly suppressed [Fig. 1(a)]. The coefficient depends on temporal memory, not on the instantaneous force distribution.

Detuned control. The previous two controls show that the kernel is memory-dependent and suppressed by the matched coarse-graining step. They do not rule out that any wave-like template swept through turbulence would produce a comparably large signal. To test channel specificity, we shift the probe carrier to $\omega_\perp = \omega(1 + \sqrt{2})$ while keeping the modal projection $e^{-i\varphi}$ in Eq. (4) at the target frequency ω. The carrier and projection are now deliberately mismatched. At $k = 10$ the SVF-to-detuned ratio exceeds $900\times$ [Fig. 1(b), Table II]. The large kernel requires matched probe-channel alignment and is not a generic property of arbitrary wave-like templates applied to turbulence. The three controls together establish that the measured two-time coherence is memory-dependent, channel-specific, and operationally suppressed by a phase-averaging surrogate. These controls isolate microscopic properties that macroscopic end-to-end validation cannot resolve.

The revealed kernel is finite and integrable (Fig. 2).—Having established that the revealed signal is channel-specific and memory-bearing, we quantify the kernel itself. The normalized autocorrelation $C_F(\tau)/C_F(0)$ decays from unity to zero at all three tested wavenumbers (Fig. 2). The Hilbert envelope decays smoothly on a timescale $\tau_{\mathrm{int}} \approx 0.019$–$0.021$, with little dependence on k, yielding about 480–530 segments per 10-second record. The Eulerian Green–Kubo coefficient from Eq. (7) is approximately constant across the three wavenumbers at $\Gamma_{\mathrm{GK}}^{\mathrm{Eul}} \approx 2.3$ [Fig. 2]. Across the 200 sampled positions the coefficient of variation is 0.70–0.72, and the standard error of the ensemble mean is about 5%. The coefficient is finite and reproducible at the ensemble level despite strong spatial intermittency.

Its approximate constancy across k is a property of the Eulerian observable. Fixed-point sampling integrates over all spatial wavenumbers q with Euler-frame decorrelation weights and therefore cannot resolve the resonant band $q \sim k$. Probe-frequency independence across 14 values of g_{ref} spanning two orders of magnitude confirms that $\Gamma_{\mathrm{GK}}^{\mathrm{Eul}}$ is a bath transport property, not a probe artifact (see Supplemental Material [19]). The mild uptick at low g_{ref} is quantitatively accounted for by the $S_W(2\omega)$ correction from the one-component carrier structure.

Sweep-influenced decorrelation from trajectory sampling (Fig. 3).—In the ocean, the wave group traverses the turbulent surface layer at speed c_g, introducing a sweep timescale $\tau_{\mathrm{sweep}} \sim \ell/c_g$, the wave-propagation analogue of Kraichnan–Tennekes random sweeping [20, 21]. In fixed-point sampling, decorrelation is set by eddy self-advection and is independent of c_g.

We first verify that fixed-point decorrelation does not depend on c_g. Scanning the same four δ values at fixed positions does not change τ_{int}. This null result confirms that probe motion, not the prescribed wave carrier, governs moving-frame decorrelation. Trajectory sampling behaves differently. The envelope decorrelation time decreases from 0.012 at $c_g = 1.8$ to 0.002 at $c_g = 17.9$ [Fig. 3(a)]. A power-law fit gives

$$\tau_{\mathrm{int}} \propto c_g^{-0.67 \pm 0.08}. \tag{9}$$

This excludes pure self-advection (c_g^0) at more than 8σ and ideal sweep (c_g^{-1}) at more than 4σ. The DNS therefore sits in a mixed decorrelation regime. Sweep is real and measurable, but not asymptotically pure at $\mathrm{Re}_\lambda \approx 433$ and $\delta = 0.01$–0.1. Trajectory sampling also suppresses serial dependence. The closure parameter drops from 3–6 at fixed points to 1.1–1.8 on moving trajectories [Fig. 3(b)]. c_0 decreases monotonically with decreasing δ, reaching 1.1 at $\delta = 0.01$. In the ocean, $\delta \sim 10^{-3}$. The observed monotonic trend and its clear physical mechanism are consistent with the $c_0 = 1$ independent-encounter baseline, though they do not by themselves prove it.

Independent satellite swell data [12] give $c_{0,\mathrm{MLE}} = 0.78 < 1$. Isotropic DNS cannot produce $c_0 < 1$ because it lacks organized spatial structure. In the ocean, Langmuir circulations impose alternating-sign vorticity along the propagation path [11], generating negative serial correlations that reduce c_0 below unity. A synthetic test illustrates this mechanism (Supplemental Material [19]). The DNS captures the sweep-driven approach to $c_0 = 1$ from above. The oceanic departure below unity is consistent with organized structure absent in isotropic turbulence.

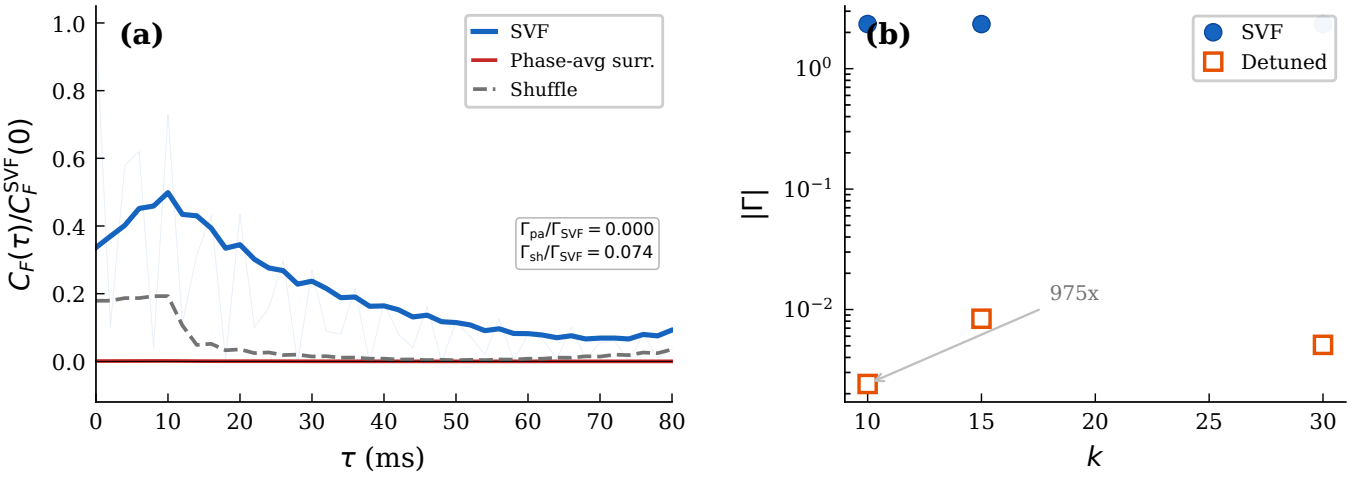

Figure 1: **Three controls establishing channel specificity, memory dependence, and phase-averaging suppression.** Same 200-position dataset at $k = 10$ (alias-free for both SVF and detuned frequencies). **(a)** $C_F(\tau)$ normalized by the SVF zero-lag value $C_F^{\mathrm{SVF}}(0)$, with Hilbert envelope shown. Blue: SVF channel. Red: phase-averaging surrogate (low-pass filtered below ω). Gray: time-shuffled record. Raw carrier oscillation shown lightly behind the SVF curve. All three curves share the same normalization, so the surrogate and shuffle amplitudes reflect the absolute suppression. Phase averaging suppresses the kernel by more than 99% ($\Gamma_{\mathrm{surr}}/\Gamma_{\mathrm{SVF}} < 0.01$). Time shuffling destroys all temporal memory. **(b)** $|\Gamma|$ versus k. Filled circles: SVF channel. Open squares: detuned control ($\omega_\perp = (1+\sqrt{2})\omega$). At $k = 10$ the ratio exceeds 900× (alias-free). Higher-k ratios are affected by aliasing (Appendix).

We note that the scaling $\tau_{\mathrm{int}} \propto c_g^{-\alpha}$ is a generic property of any observable sampled along a moving trajectory in turbulence. Its physical relevance to the SVF channel is conditional on the channel specificity established by the fixed-point controls above. Given that the measured two-time coherence belongs to the SVF channel, the c_g-dependence of its decorrelation time quantifies whether successive wave-eddy encounters are near-independent.

The per-encounter increments are nearly symmetric but strongly non-Gaussian, with kurtosis of order 10–17 (see Supplemental Material [19] for details). This intermittency does not overturn the leading Gaussian closure used at path level. It identifies the dominant correction at encounter scale.

Discussion.—The main message of this work is not that turbulence contains yet another correlation function. It is that a transport channel can be physically latent in Navier–Stokes turbulence and yet be removed from the effective description by coarse-graining. By inserting a moving wave probe, we make that latent bath-side memory appear as a finite, channel-specific friction kernel.

The probe shows that the discarded SVF fluctuation carries a measurable Green–Kubo kernel that depends on temporal memory. At $k = 10$, the detuned control suppresses the signal by more than two orders of magnitude, confirming that the large response requires matched probe-channel alignment. The result links a formal statement from nonequilibrium statistical mechanics to a concrete measurement in turbulence at $\mathrm{Re}_\lambda \approx 433$.

The trajectory scaling is not by itself specific to the SVF channel. It becomes physically meaningful only after the fixed-point controls have established channel specificity. The DNS gives $c_0 \approx 1.1$–1.8 whereas satellite data give $c_{0,\mathrm{MLE}} = 0.78$. Isotropic DNS lacks the organized spatial structure needed to drive negative serial correlations, so its c_0 should be read as an upper bound rather than an oceanic prediction.

The quantity measured here, $\Gamma_{\mathrm{GK}}^{\mathrm{Eul}}$, is an existence diagnostic for the selected channel, not a direct estimate of the oceanic attenuation coefficient μ_E. The present protocol is general. The companion paper [12] applies a closure to the same underlying channel and derives the parameter-free swell attenuation law validated against 241 trans-oceanic satellite tracks. The two papers are complementary rather than sequential. The companion derives the closed-form law for a specific, closure-reducible case. The present paper establishes the general detection framework within which such kernels can be identified before any closure is imposed.

The broader implication is methodological. Coarse-graining often removes a bilinear coupling between a fast wave and a slow stochastic bath at the one-time level. When it does, a moving wave probe can test whether a finite two-time response survives before any closure is imposed. The protocol is indifferent to the specific wave type, bath dynamics, or closure scheme. Surface swell in a turbulent upper ocean is the demonstrated instance. Internal gravity waves in vortical flow, atmospheric gravity

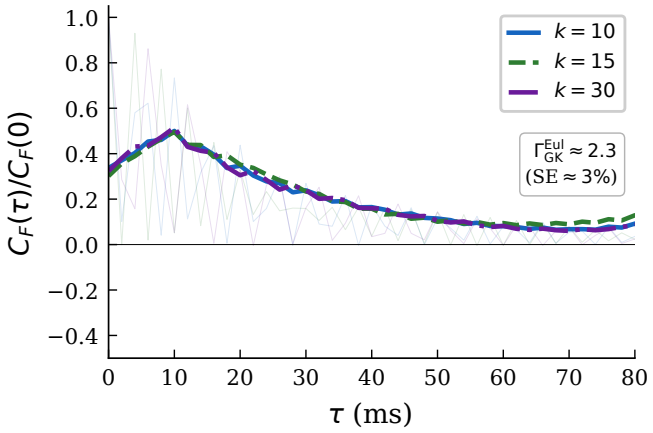

Figure 2: **SVF friction kernel: existence and integrability.** The `isotropic1024coarse` dataset with $\mathrm{Re}_\lambda \approx 433$ and $\varepsilon = 0.093$ is queried at 200 fixed positions over 5028 frames with $\Delta t = 0.002$. A kinematic probe with $g_{\mathrm{ref}} = 38{,}269$ is applied at $k \in \{10, 15, 30\}$. Normalized $C_F(\tau)/C_F(0)$ averaged over 200 positions. Light curves: raw signal. Solid curves: Hilbert envelope. The $\cos^2(\omega\tau)$ oscillation is carrier self-mixing from the one-component probe. The smooth envelope is the operational extraction of bath-side decorrelation. Integrating $\mathrm{Re}\, C_F$ over the envelope-defined window yields $\Gamma_{\mathrm{GK}}^{\mathrm{Eul}} \approx 2.3$ (DNS units), finite and reproducible at the 5% level across 200 positions.

waves in turbulence, Alfvén waves in magnetized plasma, and acoustic waves in strongly fluctuating flows share this structure. Each is a natural testing ground for the protocol.

The probe is kinematic, the DNS bath is isotropic with no free surface, and the one-component carrier requires operational demodulation. These simplifications isolate the channel-selection problem from the full wave–turbulence interaction. Phase-resolved coupled DNS [22] and rapid-distortion approaches [23] would bridge the gap to fully dynamical wave–eddy coupling. Recent work on directional scattering of wave action by macroturbulence [24] addresses a complementary aspect of the same problem.

The kernel reported here is not a pre-existing object in bare turbulence. What is pre-existing is the bath-side memory and the capacity of that memory to support a channel-specific response. The probe converts that latent memory into an operationally measurable friction kernel. Whenever a fast-oscillating coupling is phase-averaged out of an effective theory, the same procedure can test whether the corresponding transport channel survives.

We acknowledge the Johns Hopkins Turbulence Database and SciServer for providing public access to the DNS datasets. This work was supported by Khalifa University of Science and Technology, Abu Dhabi, UAE.

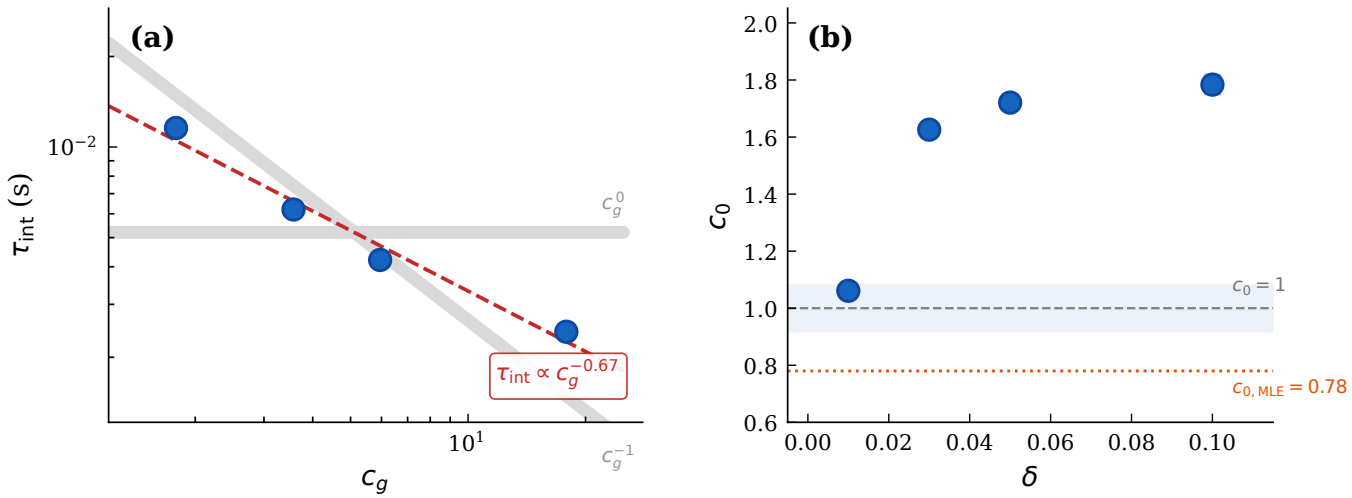

Figure 3: **Sweep-influenced decorrelation from trajectory sampling.** $k = 30$, 50 trajectories per δ, advancing at $c_g\,\hat{\boldsymbol{x}}$ (mod 2π). **(a)** τ_{int} versus c_g in log–log form. Light bands: reference slopes c_g^0 (self-advection) and c_g^{-1} (pure sweep). Red dashed fit: $c_g^{-0.67\pm0.08}$, excluding both limits. **(b)** Closure parameter c_0. Dashed line: $c_0 = 1$ (independent encounters). Dotted line: $c_{0,\text{MLE}} = 0.78$ from satellite data. DNS values remain $O(1)$ throughout.

* guoqiang.liu@ku.ac.ae

[1] M. S. Green, Markoff random processes and the statistical mechanics of time-dependent phenomena. II. irreversible processes in fluids, J. Chem. Phys. **22**, 398 (1954).

[2] R. Kubo, Statistical-mechanical theory of irreversible processes. I. general theory and simple applications to magnetic and conduction problems, J. Phys. Soc. Jpn. **12**, 570 (1957).

[3] R. Kubo, The fluctuation-dissipation theorem, Rep. Prog. Phys. **29**, 255 (1966).

[4] H. Mori, Transport, collective motion, and Brownian motion, Prog. Theor. Phys. **33**, 423 (1965).

[5] R. Zwanzig, *Nonequilibrium Statistical Mechanics* (Oxford University Press, 2001).

[6] D. G. Andrews and M. E. McIntyre, An exact theory of nonlinear waves on a Lagrangian-mean flow, J. Fluid Mech. **89**, 609 (1978).

[7] A. D. D. Craik and S. Leibovich, A rational model for Langmuir circulations, J. Fluid Mech. **73**, 401 (1976).

[8] S. Leibovich, The form and dynamics of Langmuir circulations, Annu. Rev. Fluid Mech. **15**, 391 (1983).

[9] O. Bühler, *Waves and Mean Flows*, 2nd ed. (Cambridge University Press, 2014).

[10] J. C. McWilliams, Surface wave effects on submesoscale fronts and filaments, J. Fluid Mech. **951**, A21 (2022).

[11] J. C. McWilliams, P. P. Sullivan, and C.-H. Moeng, Langmuir turbulence in the ocean, J. Fluid Mech. **334**, 1 (1997).

[12] G. Liu and M. Al Alshehhi, Fluctuation-induced dissipation for ocean surface waves, submitted (2026).

[13] H. Jiang, A. Mironov, L. Bian, R. Morrow, and B. Chapron, Tracking the attenuation and nonbreaking dissipation of swells using altimeters, J. Geophys. Res. Oceans **121**, 1446 (2016).

[14] J. E. Stopa, F. Ardhuin, and F. Collard, Swell dissipation from 10 years of Envisat advanced synthetic aperture radar in open oceans, Geophys. Res. Lett. **43**, 3423 (2016).

[15] F. E. Snodgrass, G. W. Groves, K. F. Hasselmann, G. R. Miller, W. H. Munk, and W. H. Powers, Propagation of ocean swell across the Pacific, Philos. Trans. R. Soc. London, Ser. A **259**, 431 (1966).

[16] F. Ardhuin, B. Chapron, and F. Collard, Observation of swell dissipation across oceans, Geophys. Res. Lett. **36**, L06607 (2009).

[17] Y. Li, E. Perlman, M. Wan, Y. Yang, C. Meneveau, R. Burns, S. Chen, A. Szalay, and G. Eyink, A public turbulence database cluster and applications to study Lagrangian evolution of velocity increments in turbulence, J. Turbul. **9**, N31 (2008).

[18] E. Perlman, R. Burns, Y. Li, and C. Meneveau, Data exploration of turbulence simulations using a database cluster, Proc. ACM/IEEE SC 2007 , 1 (2007).

[19] See Supplemental Material at [URL] for envelope sensitivity, per-position statistics, encounter closure sensitivity, phase-averaging surrogate details, frames per encounter, encounter intermittency, probe-frequency scan, and synthetic Langmuir roll test.

[20] R. H. Kraichnan, Kolmogorov's hypotheses and Eulerian turbulence theory, Phys. Fluids **7**, 1723 (1964).

[21] H. Tennekes, Eulerian and Lagrangian time microscales in isotropic turbulence, J. Fluid Mech. **67**, 561 (1975).

[22] A. Xuan, B.-Q. Deng, and L. Shen, Turbulence and wave interaction in the presence of wind shear, J. Fluid Mech. **980**, A12 (2024).

[23] M. A. C. Teixeira and S. E. Belcher, On the distortion of turbulence by a progressive surface wave, J. Fluid Mech. **458**, 229 (2002).

[24] A. B. Villas Bôas and W. R. Young, Directional diffusion of surface gravity wave action by ocean macroturbulence, J. Fluid Mech. **890**, R3 (2020).

End Matter

Nyquist analysis and detuned controls at all k

The Nyquist frequency for the DNS time step $\Delta t = 0.002$ is $\omega_N = \pi/\Delta t \approx 1571$. For the SVF probe at $g_{\text{ref}} = 38\,269$, the probe frequencies are $\omega(k) = \sqrt{g_{\text{ref}} k}$. Table I lists ω, the Nyquist margin ω/ω_N, and the detuned control frequency $\omega_\perp = (1+\sqrt{2})\,\omega$ for each candidate k. Wavenumbers $k = 55$ and $k = 80$ are excluded because $\omega/\omega_N > 0.85$.

Table I: Nyquist safety and detuned control frequencies ($g_{\text{ref}} = 38\,269$, $\omega_N \approx 1571$).

k	ω	ω/ω_N	$\omega_\perp$	$\omega_\perp$ aliases?
10	619	0.39	1493	No
15	758	0.48	1829	Yes
30	1071	0.68	2587	Yes
55	1451	0.92	3503	Yes
80	1750	1.11	4224	Yes

For $k \geq 15$, the detuned frequency $\omega_\perp$ exceeds ω_N and aliases to an effective frequency within the resolved band. The measured SVF-to-detuned ratio at higher k is therefore affected by aliasing and reported with this caveat.

Table II: SVF-to-detuned ratio at each tested wavenumber (200-position ensemble mean, $\alpha = 1+\sqrt{2} \approx 2.414$).

k	$\lvert\Gamma^{\text{Eul}}_{\text{GK}}\rvert_{\text{SVF}}$	$\lvert\Gamma\rvert_{\text{det}}$	Ratio
10	2.35	2.4×10^{-3}	975×
15	2.35	8.4×10^{-3}	280×
30	2.34	5.1×10^{-3}	461×

All ratios exceed 280×. The variation across k reflects aliasing geometry, which can increase or decrease the apparent detuned leakage depending on the Nyquist fold.